科学通报 2017 年 第 62 卷 第 7 期: 711 ~ 720
论 文
《中国科学》杂志社
SCIENCE CHINA PRESS

# 伊豆-小笠原地区岩石圈软流圈边界地震学证据

崔辉辉[1,2], 高雅健[1,2], 周元泽[1,2*]

1. 中国科学院计算地球动力学重点实验室, 北京 100049;
2. 中国科学院大学地球科学学院, 北京 100049
* 联系人, E-mail: yzzhou@ucas.ac.cn, yzzhou@gmail.com

2016-10-08 收稿, 2016-11-09 修回, 2016-11-10 接受, 2017-02-10 网络版发表
国家自然科学基金(41274092, 41474070)资助

**摘要** 岩石圈软流圈边界(lithosphere-asthenosphere boundary, LAB)是上地幔内具有负速度梯度的地震间断面. 开展对俯冲带区域LAB的地震学探测有助于进一步理解岩石圈与软流圈的相互作用以及与板块俯冲相关的地球动力学过程. 本文收集了2002~2014年发生于伊豆-小笠原地区的3个深源地震(400~600 km)的垂向宽频带波形资料, 利用线性倾斜叠加方法对波形数据进行处理后获得了相对走时-慢度域的灰度图和叠加波形图, 并成功提取了*sP*震相在LAB反射的前驱震相$s_{LAB}P$, 该震相的极性与*sP*相反, 幅度比为0.17~0.21. 基于改进的一维速度模型IASP91-IB计算获得了近源区6个$s_{LAB}P$震相反射点的分布. 研究表明伊豆-小笠原岛弧下方LAB深度位于58~65 km, 平均深度为62 km, 起伏变化较小(7 km). 与菲律宾海构造稳定地区研究结果相比, 伊豆-小笠原岛弧地区海洋岩石圈出现了明显减薄的现象, 其应与西太平洋俯冲板块在地球深部持续释放的挥发分物质导致了软流圈出现部分熔融以及弧后地幔楔内小尺度对流的强侵蚀作用密切相关.

**关键词** 岩石圈软流圈边界, 伊豆-小笠原地区, 俯冲带, *sP* 前驱震相, 线性倾斜叠加

岩石圈软流圈边界(lithosphere-asthenosphere boundary, LAB)是地球内部相对刚性的岩石圈和黏塑性软流圈之间的分界面[1~3], 其性质也被认为是理解板块构造理论的重要基础[3,4]. 作为上地幔中力学性质发生明显变化的界面, LAB的存在形态关系到岩石圈与软流圈之间的解耦(decoupling)程度[5,6], 对于板块汇聚或海洋岩石圈向地球深部俯冲[7]的地质构造过程具有重要的影响. 对LAB开展地震学精细探测有助于进一步认识地幔对流、板块运动以及岩石圈演化等地球动力学过程.

地震学上通常将上地幔地震波低速区(low velocity zone)作为软流圈出现的标志[1,8,9], 其低速特征一般被认为与地幔物质部分熔融(partial melting)或者脱水(dehydration)等因素有关[5]. LAB在深度方向上为大陆或海洋岩石圈的高速向软流圈的低速变化的过渡区间[3]. 相比于大陆岩石圈, LAB在年轻的海洋岩石圈下方更为明显[10]. 地震学研究显示海洋板块下方LAB为一尖锐(<20 km)且具有明显地震波速度降(5%~10%)的间断面, 其深度位于35~120 km[8,11~13]. 在远离俯冲带或地幔柱活动的海洋地区, 岩石圈厚度与洋壳年龄呈现出正相关的趋势[11,14]. 热地幔物质上涌, 小尺度地幔对流和板块俯冲等地球动力学过程引发的流体释放可导致地幔物质出现部分熔融, 进而局部地增大LAB的地震波反射率[5,13].

目前对海洋地区LAB特征的研究取得了一些成果, 但海洋俯冲带区域LAB的探测结果并不多见, 主要是因为布设和维护海底地震仪的成本很高, 不宜在海底进行大面积高密度覆盖观测, 因此近台站*Ps*/*Sp*

**引用格式**: 崔辉辉, 高雅健, 周元泽. 伊豆-小笠原地区岩石圈软流圈边界地震学证据. 科学通报, 2017, 62: 711–720
Cui H H, Gao Y J, Zhou Y Z. Seismic evidence of the lithosphere-asthenosphere boundary beneath Izu-Bonin area (in Chinese). Chin Sci Bull, 2017, 62: 711–720, doi: 10.1360/N972016-00889

转换震相[15~18]的应用受到了台站覆盖的限制; 常用于地球深部间断面研究的*ScS*混响(reverberations)[10,19,20]以及长周期*PP*/*SS*前驱震相[13,21]的采样区域对震源和台站的分布位置要求较高. 近源次生震相对俯冲带附近间断面的结构能提供有效的约束[22~26], 其中地表强反射震相(如*sP*, *pP*和*sS*)的前驱波可应用于震源上方间断面的探测[27~30].

伊豆-小笠原地区位于菲律宾海板块的东北部, 长期受到西太平洋板块的俯冲作用并发育有经受拉张作用的伊豆-小笠原岛弧(Izu-Bonin Arc)[31]. 该地区是LAB研究的盲点地区之一, 其周边区域陆续有关于LAB存在形态的报道. Kato和Jordan[20]利用*ScS*混响和横波及面波观测资料的联合反演得出了西菲律宾海(Western Philippine Sea)地区一维PHB3模型, 显示LAB是一深度在89 km的尖锐速度跃变界面, 其附近的地震波速度降为3.6%. Kawakatsu等人[11]利用钻孔地震台(borehole station)的接收函数研究也揭示了菲律宾海中部地区下方LAB的尖锐(10~15 km)和负速度比(7%~8%)的特征, 其中洋壳年龄为49 Ma的西菲律宾海盆(West Philippine Basin, WPB)下方LAB深度为76±1.8 km, 洋壳年龄为25 Ma的帕里西维拉海盆(Parece Vela Basin, PVB)下方LAB的深度为55 km. Kumar和Kawakatsu[14]进一步确认了北太平洋板块边界地区海洋岩石圈的厚度随着洋壳年龄的增大而变大的趋势.

本文选用位于美国中西部地区的部分高密度固定地震台网和流动台阵所记录到的伊豆-小笠原地区3个深源地震的垂向宽频带波形资料, 利用线性倾斜叠加方法提取了*sP*在LAB反射的前驱震相$s_{\mathrm{LAB}}P$, 对伊豆-小笠原地区LAB的性质与起伏形态进行了小尺度研究. 通过与菲律宾海其他地区LAB研究结果的对比, 本文对西太平洋板块俯冲相关的构造活动对该地区岩石圈的影响进行了探讨与分析.

## 1 资料选取与处理

*sdP*震相表示离源上行的*S*波在遇到震源上方间断面(深度为*d*)时反射并转换为下行*P*波, 即*sP*的前驱震相(图1). 相比于近台站*Ps*/*Sp*转换震相和长周期*PP*/*SS*前驱震相, 近源震相的菲涅尔区(Fresnel zone)较小, 因此对地球内部结构的分辨率更高一些[32~34]. 深震资料的强反射震相*sP*与*pP*之间具有足够长的走时空窗, *sdP*震相不会受到*pP*及其地壳内多次反射波的干扰. *sP*及其前驱震相射线路径差别主要集中在地表与间断面之间(图1), 两震相的走时差与慢度差可有效应用于震源上方间断面的形态特征研究[27,28]. 由于*sdP*震相自身能量较弱, 可能会受到背景噪声的干扰而不容易在观测波形中被直接识别出来, 因此本文采用线性倾斜叠加方法来增强信号的强度. 线性倾斜叠加是*N*次根倾斜叠加方法(*N*-th root stack method)[23~25,35,36]和相位加权叠加方法(phase-weighted stack method)[33,37]的特殊形式, 其优点在于数据叠加过程中不会产生波形畸变的现象[26,37], 可以较好地评价次生震相的振幅特性.

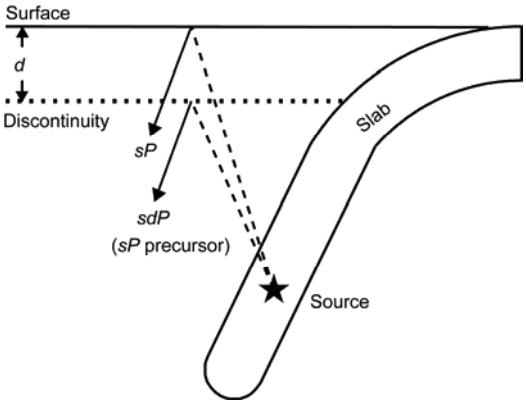


**图 1** *sP*及其前驱震相*sdP*示意图. 射线路径上虚线为*S*波, 实线为*P*波. *sdP*震相为上行*S*波在间断面底反射并转换为下行*P*波

**Figure 1** The schematic illustration describing the *sP* phase and its precursor (*sdP*). The dashed and solid lines denote the *S* and *P* waves in ray paths, respectively. The *sdP* phase is the underside reflection and conversion of an upgoing *S* wave to a downgoing *P* wave on a discontinuity

本文收集了2002~2016年发生于伊豆-小笠原地区的深源地震事件(400~600 km, $M_{\mathrm{w}}$>6.0), 选用了固定台网和流动台阵所记录的远震中距(80°~100°)垂向宽频带波形资料, 地震数据下载于美国地震学研究联合会(Incorporated Research Institutions for Seismology, IRIS)网站(http://www.iris.edu/). 本文选用的固定台网包括美国的CI台网和ANZA台网, 流动台阵则包括美国USArray(2010年)中的TA台阵和YX流动台阵(图2(a)). 考虑到台站分布情况同时更有效地利用地震数据来探测速度界面可能的横向变化, 本文将CI和ANZA台网合并为子台网CZ(图2(b)), 并将TA台阵划分为子台网TA1和TA2(图2(c)). 采用高密度的台站可使得台网/台阵具有很小的方位角范围, 同时对应的*sP*震相在近源区反射点的分布是比较集中的(图2(a); CZ, 10.0 km×8.9 km; TA1, 16.6 km×

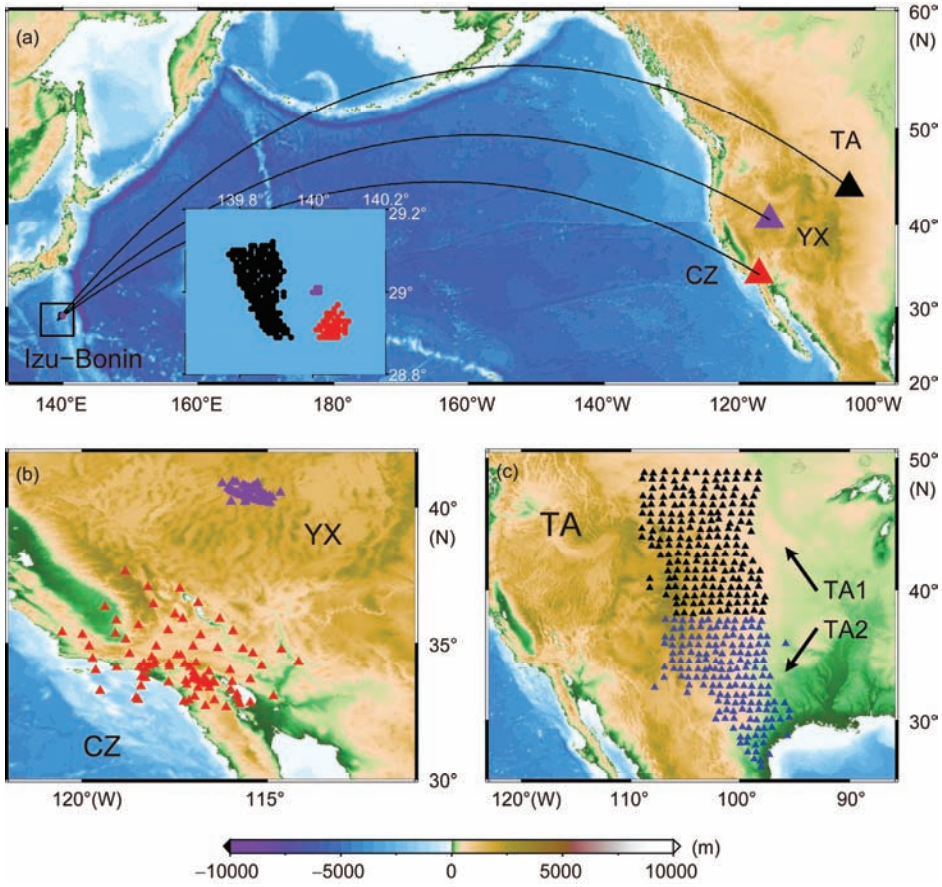


**图 2** 震源至台站的形状(a)和各子台网的台站分布图((b), (c)). (a) 矩形表示震中位置, 三角形表示台网/台阵分布, 黑色实线为*sP*震相射线路径的地表投影, 彩色圆点为*sP*地表反射点分布. (b) 紫色和红色三角形分别为子台网YX和CZ. (c) TA台阵划分为子台网TA1(黑色三角形)和TA2(蓝色三角形). 背景图中海底测深和陆地地形的数据引自ETOPO1 模型[38]

**Figure 2** The source-receiver geometry (a) and station distributions of the sub-networks ((b), (c)). (a) The rectangle denotes the epicenter location, the triangles denote the network/array distributions, and the black lines are the horizontal projections of ray paths for *sP* phases, with the reflected points on the surface marked by the colored circles. (b) The purple and red triangles denote the sub-networks YX and CZ, respectively. (c) The stations of TA are divided into the sub-networks TA1 (black triangles) and TA2 (blue triangles). The ocean bathymetry and land topography data for background images are taken from the ETOPO1 model[38]

18.9 km; TA2, 12.2 km×8.9 km; YX, 2.2 km×1.1 km), 因此可明显降低台站方位角以及台站分布对反射点位置的影响.

从收集的地震事件中仔细挑选出*sP*震相持续时长小于15~20 s且信噪比足够好的3个地震事件, 共计6个地震事件-子台网分组(表1). 震源参数引自美国地质调查局(US Geological Survey)发布的PDE (Preliminary Determination of Epicenters)目录(http://earthquake.usgs.gov/data/pde.php), 震源机制解参数引自全球质心矩张量解(Global Centroid-Moment-Tensor, GCMT) (http://www.globalcmt.org/)[39,40].

本文的资料处理主要步骤包括: (1) 对原始地震数据进行去均值、去线性趋势以及去仪器响应处理. (2) 通过对地震数据进行Fourier频谱分析确定出适用于*sP*震相的最佳滤波窗为0.01~0.2 Hz, 并进行带通滤波处理. (3) 对各分组的波形以*sP*震相的峰值点对齐并归一化, 选取信噪比最好的60道数据进行线性倾斜叠加处理(如果子台网挑选后的波形数据小于60道, 则全部用于处理)得到叠加波形, 观测和合成波形示例见图3. (4) 将叠加波形数据进行Hilbert变换获得包络线, 进一步做10为底的对数并乘以20倍的处理, 绘制相对走时-慢度域的灰度图(vespagram). (5) 考虑到浅部速度结构对*sP*震相射线路径的影响[28], 本文利用CRUST1.0模型[42]对IASP91参考模型[43]的浅部地壳速度结构进行改进, 得到了IASP91-IB模型(图4). 利用TauP程序[44,45]基于该改进模型计

**表 1** 本文所用地震事件和$s_{LAB}P$震相反射深度列表[a)]

**Table 1** Earthquakes used and reflected depths of the $s_{LAB}P$ phases

| 事件 | 发震时刻UTC | 深度 (km) | 震中 Lat, Lon | 震级 ($M_w$) | 子台网 | 震中距 (°) | 反射点 Lat, Lon | LAB深度 (km) |
|---|---|---|---|---|---|---|---|---|
| 1 | 2002-08-02 23:11:39.13 | 426.1 | 29.280°N, 138.970°E | 6.3 | CZ | 84.38 | 29.65°N, 139.86°E | 58 |
| 2 | 2010-11-30 03:24:40.18 | 470.0 | 28.349°N, 139.187°E | 6.8 | CZ | 84.76 | 28.94°N, 140.09°E | 62 |
| | | | | | TA1 | 87.78 | 29.07°N, 139.88°E | 65 |
| | | | | | TA2 | 95.88 | 28.96°N, 139.91°E | 61 |
| | | | | | YX | 82.53 | 29.04°N, 140.05°E | 64 |
| 3 | 2014-06-30 19:55:32.39 | 511.0 | 28.340°N, 138.844°E | 6.2 | CZ | 85.07 | 28.94°N, 139.78°E | 62 |

a) CZ为Caltech Regional Seismic Network (CI)和ANZA Regional Network (ANZA)的合并子台网，共85个地震台；TA是Transportable Array的缩写，共407个地震台，划分为子台网TA1和TA2；YX是Flexarray 3D Passive Seismic Imaging of Core-Complex Extension in the Ruby Range Nevada的缩写，共50个地震台

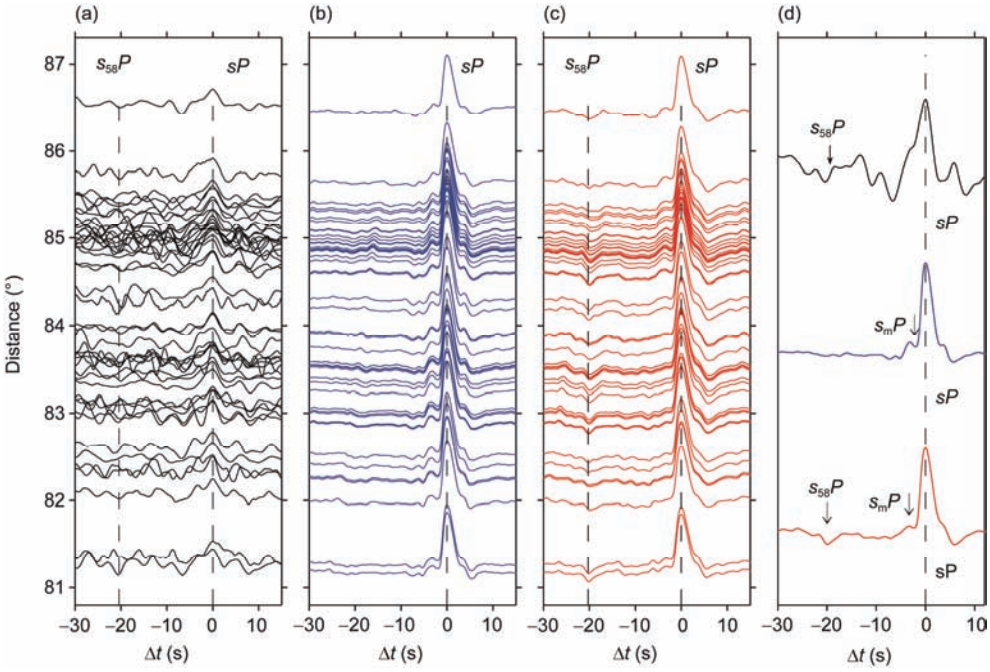


**图 3** 子台网CZ记录的地震事件 1 的观测波形和合成波形. (a) 观测波形; (b) 基于IASP91-IB模型以反射率法[41]计算的合成波形; (c) 在IASP91-IB模型中添加尖锐的LAB(深度 58 km, 速度降为 5%)的合成波形; (d) (a)~(c)中波形的叠加结果

**Figure 3** Observed waveforms of Event 1 recorded by the sub-network CZ and synthetic waveforms. (a) Observed waveforms; (b) synthetic waveforms with the reflectivity code[41] calculated with the IASP91-IB model; (c) synthetic waveforms calculated with the IASP91 model added the sharp LAB at 58 km with the velocity decrease of 5%; (d) stacked results of the waveforms in (a)–(c)

算*sdP*相对于*sP*的理论走时差和慢度差分布，在此基础上综合灰度图和叠加波形图进行次生震相的识别. (6) 计算所识别次生震相的反射点水平和深度分布. 更为详细的倾斜叠加原理分析与数据处理过程请参见臧绍先和周元泽[26].

反射点深度误差主要来自次生震相的走时拾取误差和俯冲板块高速异常引起的走时偏差. 手动拾取次生震相的走时误差一般控制在0.5 s之内[46], 以IASP91-IB模型换算后深度误差大致为2.0 km. 俯冲板块的局部速度异常造成的深度误差在1 km之内, 对反射点水平位置造成的误差在5~10 km[22]. 对于深源地震而言，震源深度的定位误差对*sdP*和*sP*之间走时差及慢度差的影响很小，对反射点水平位置造成的误差小于10 km[22]. 因此最后得出所确定的反射点深度误差大致在3 km之内，水平位置不确定性大致小于15~20 km.

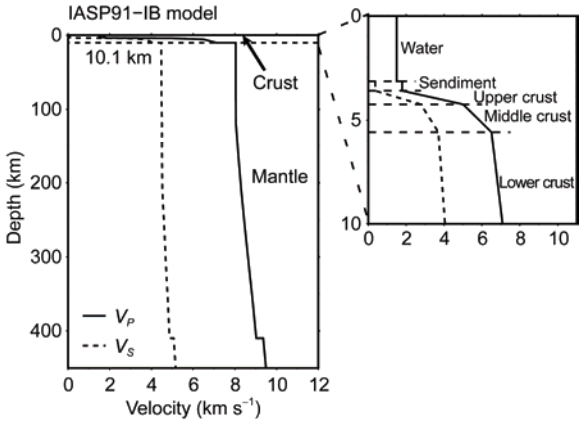


**图 4** 伊豆-小笠原地区IASP91-IB模型的*P*波和*S*波速度图. 地壳部分速度引自CRUST1.0模型[42](右侧放大图像), 地幔部分引自IASP91模型[43]. 实线和虚线分别为*P*波和*S*波速度

**Figure 4** *P*- and *S*-wave velocities of the IASP91-IB model for Izu-Bonin area. The velocities of the crust part (enlarged image on the right) are from the CRUST1.0 model[42], and the ones of the mantle part are from the IASP91 model[43]. The solid and dashed lines denote *P*- and *S*-wave velocities, respectively

## 2 研究结果

图5给出了6个地震事件-子台网分组的线性倾斜叠加灰度图, 可以看出*sP*震相的持续时长约为20 s, 0 s时刻对应于*sP*震相的峰值点因而能量最强. 由*sdP*相对于*sP*的理论走时差和慢度差分布(图5中绿色实线)可看出*sdP*与*sP*的慢度差较小, 在此理论变化趋势的一定慢度范围内的震相可认为是*sdP*震相. 基于IASP91-IB模型, 6个地震事件-子台网分组的叠加波形经时深转换(time-to-depth conversion)计算得到偏移结果(图6), 所标注的次生震相对应于叠加灰度图(图5)中所识别的次生震相.

由图5(a)~(f)中可见, 次生震相整体上分布较少, 这有利于震相识别. 在*sP*震相前20~24 s之间均存在一个明显的次生震相, 其相对慢度−0.15~0.10 s deg$^{-1}$, 与*sP*震相的慢度较为接近, 经时深转换计算后得出的深度位于58~65 km. 选择叠加波形的时深转换结

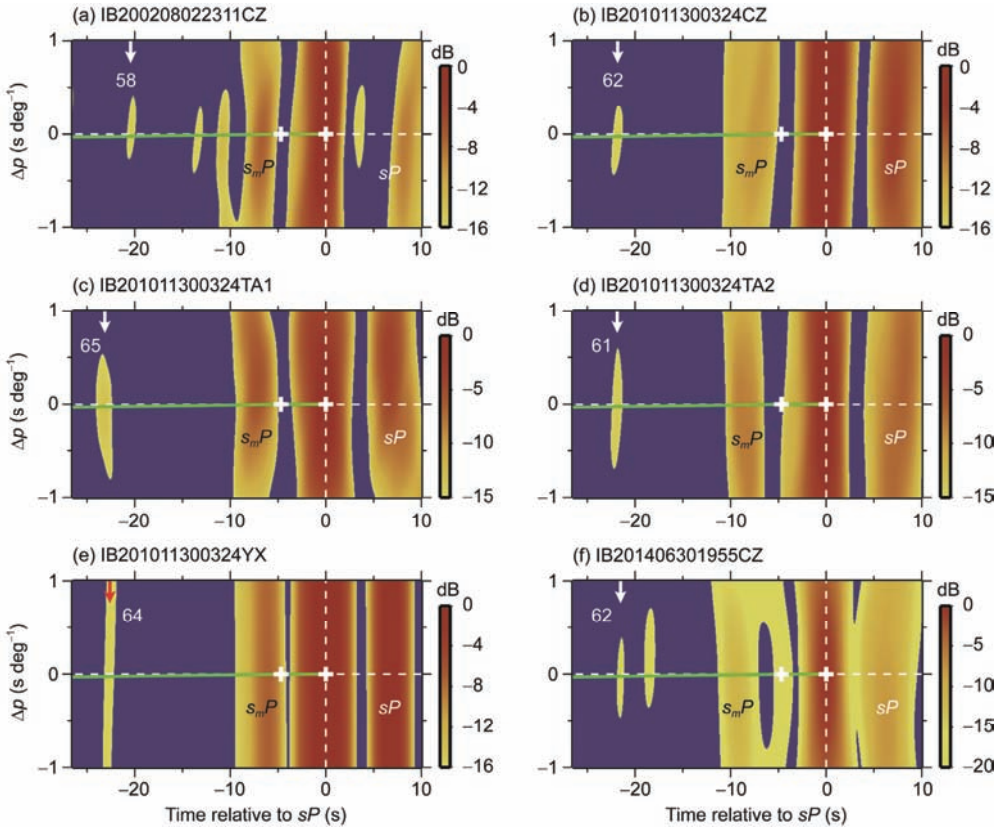


**图 5** 线性倾斜叠加灰度图. 白色加号表示基于IASP91-IB模型计算的理论*sdP*震相. 绿色线为*sdP*相对于*sP*的理论走时差和慢度差分布. 箭头指向$s_{LAB}P$震相的位置, 相应的数字为反射点深度

**Figure 5** The vespagrams of the linear slant stacks. The white pluses denote the theoretical *sdP* phases calculated with the IASP91-IB model. The green lines represent the theoretical travel-time and slowness of the *sdP* phases relative to the *sP* phases. The arrows with the numbers point to the $s_{LAB}P$ phases and their reflected depths

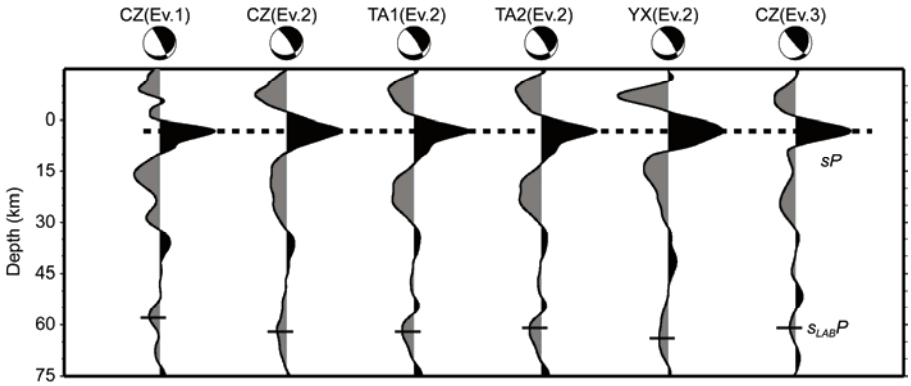


**图 6** 叠加波形的偏移结果. 横轴和纵轴分别表示震源-子台网分组和LAB深度. 填充波形的黑色表示振幅为正, 灰色表示振幅为负

**Figure 6** The migration results of the stacked waveforms. The horizontal and vertical axes are the earthquake event to sub-network pairs and the LAB depths, respectively. The black and gray colors filled in the waveforms indicate the positive and negative amplitudes, respectively

果作为对照(图6), 可以发现灰度图中的次生震相与*sP*极性相反, 相对于*sP*震相的幅度比为0.17~0.21. 与具有强烈不均匀性的大陆岩石圈相比, 海洋岩石圈的结构相对简单[8,11,13,47], 如克拉通岩石圈地区存在岩石圈内部间断面(intra-lithospheric discontinuity, ILD)[47]、岩石圈中部间断面(mid-lithosphere discontinuity, MLD)[48,49], 而海洋地区并未有ILD和MLD方面的报道. 结合菲律宾海地区的LAB研究结果(55~89 km)[11,14,19,20]以及正演测试的合成波形(图3), 可以确定所识别的次生震相为$s_{\mathrm{LAB}}P$, 由6组次生震相识别结果得出LAB平均深度为62 km, 深度起伏为7 km. 此外, 图6中CZ(Ev. 1) 68 km处存在一弱震相, 但并未在叠加灰度图(图5(a))中显示, 结合相邻的叠加结果, 选择了58 km处振幅较大的震相作为目标$s_{\mathrm{LAB}}P$次生震相.

基于IASP91-IB模型(图4)进行计算显示理论$s_mP$震相与*sP*的走时差仅为–4.7 s. 受*sP*震相持续时长(~20 s)特征的影响, $s_mP$震相会与*sP*震相混合而难以被识别出来. 与此同时, 所用地震事件的震源机制解不同导致辐射花样(radiation pattern)的差别, 或者俯冲板块残片或局部散射体对地震波传播有一定影响[46,50~52], 因而灰度图以及叠加波形图中*sdP*次生震相的能量或幅度有所差异. 图5(f)中在*sP*震相前15~20 s之间存在一次生震相, 其相对于*sP*震相的慢度差偏大(~0.35 s deg$^{-1}$), 该次生震相可能体现了地幔中的局部散射体对地震射线传播的影响[51,52].

## 3 讨论和结论

由图7(a)可以看出, 6个$s_{\mathrm{LAB}}P$次生震相反射点的地表投影位于伊豆-小笠原岛弧的中部地区, 因而本文的研究结果揭示了伊豆-小笠原岛弧下方LAB的存在特征: LAB深度位于58~65 km, 平均深度为62 km, 整体上起伏变化较小(7 km). 除LAB的深度外, 洋壳年龄也是评价海洋岩石圈所处演化状态的重要参数. 海洋钻探计划(Ocean Drilling Program, http://www-odp.tamu.edu/index.html)125航次的786点位于伊豆-小笠原岛弧的中北部地区, 岩石样品的同位素组分($^{40}$Ar/$^{39}$Ar)分析显示其年龄约为45.3 Ma[55], 因此岛弧下方的洋壳年龄属于始新世时期.

地热学上所定义的岩石圈底的温度大致在1300℃[4,56]. 受构造活动的影响, 俯冲带地区温度结构和岩石圈特征往往较为复杂[56]. 本文将LAB的研究结果与其他学者在菲律宾海地区的研究结果[11,14]作对比, 以分析不同构造区域海洋岩石圈的特征. 由图7(b)可以看出, 在远离俯冲带的西菲律宾海盆(WPB)和帕里西维拉海盆(PVB)地区, 海洋岩石圈厚度与年龄的分布在1100℃等温线附近; 在琉球海沟南部(RT1)和日本南海海槽(NT)地区, 海洋岩石圈厚度与年龄的分布在1050℃等温线附近, 而琉球海沟北部(RT2)地区可能因冲大东扩张海脊的火山活动[31]的残留影响而导致岩石圈厚度与年龄的分布在900℃等温线附近. 因而, 在构造相对稳定的地区, 海洋岩石圈底的温度偏高, LAB相对深一些; 在构造运动活跃的板块边界地区, 如海沟、海槽以及扩张海脊等, 海洋岩石圈底的温度偏低, LAB相对浅一些. 本文中伊豆-小笠原岛弧下方岩石圈的研究结果位于950℃等温线附近, 偏离1100℃等温线的幅度较日本南海海槽(NT)以及琉球海沟南部(RT1)地区稍大一些, 这

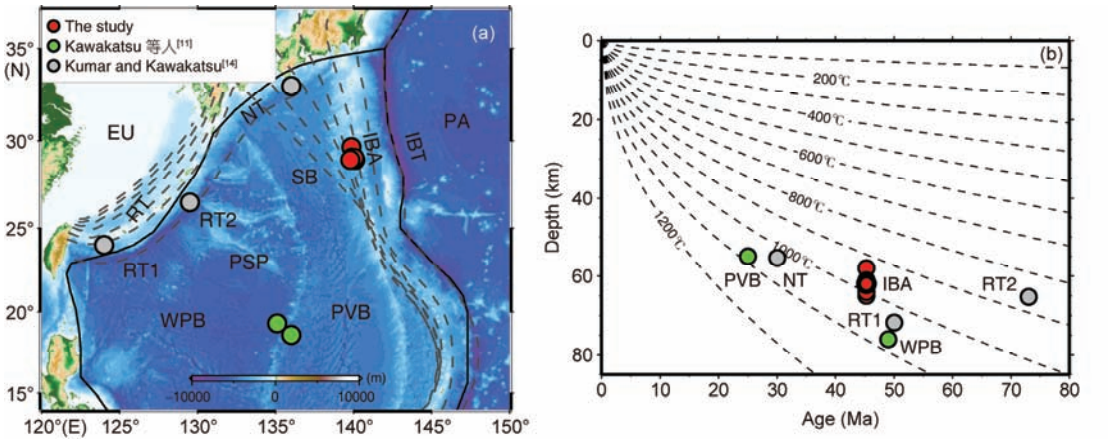


**图 7** 反射点水平分布(a)和LAB深度与洋壳年龄关系图(b). 红点为本文中反射点水平分布. 绿色和灰色点分别表示Kawakatsu等人[11]和Kumar和Kawakatsu[14]文中LAB研究结果. 灰色虚线为和达-贝尼奥夫带等深线[53]. PA, 太平洋板块; EU, 欧亚板块; PSP, 菲律宾海板块; IBT, 伊豆-小笠原海沟; RT, 琉球海沟; NT, 日本南海海槽; IBA, 伊豆-小笠原岛弧; SB, 四国盆地; PVB, 帕里西维拉盆地; WPB, 西菲律宾海盆. 等温线由半空间冷却模型[54]计算得出并以黑色虚线表示

**Figure 7** The horizontal distributions of reflected points (a) and the crustal age dependence of LAB depths (b). The red dots denote the horizontal projections of the reflected points in the study. The green and gray dots denote the results in Kawakatsu et al.[11] and Kumar and Kawakatsu[14], respectively. The contours shown in the gray dashed lines represent the Wadati-Benioff Zone[53]. PA, Pacific Plate; EU, Eurasian Plate; PSP, Philippine Sea Plate; IBT, Izu-Bonin Trench; RT, Ryukyu Trench; NT, Nankai Through; IBA, Izu-Bonin Arc; SB, Shikoku Basin; PVB, Parece Vela Basin; WPB, West Philippine Basin. The isotherms calculated with the half-space cooling model[54] are shown in black dashed lines

样的LAB起伏形态应与区域构造活动密切相关.

西太平洋板块在伊豆-小笠原海沟处向菲律宾海板块发生俯冲汇聚, 其速率为4.5~5.8 cm/a, 俯冲角度约70°~80°[57], 属于冷的俯冲板块, 弧后扩张脊发育[7]. 高分辨率地震层析成像显示太平洋板块在该区域上地幔内显示为地震波高速异常[58], 俯冲板块在地幔转换带内停滞于660 km间断面之上而形成了滞留板块(stagnant slab), 太平洋板块在日本海俯冲区也呈现出相似的滞留特征[58,59]; 而在俯冲/滞留板块上方较大范围内存在地震波低速异常, 一般认为与地幔楔(mantle wedge)内部分熔融的存在相关[58~61]. 俯冲下去的板片通过脱水作用在地球内部不同深度持续地释放水等挥发分物质, 因而引发软流圈物质出现部分熔融并且导致地幔楔内的小尺度对流变得更为活跃[58,59]. 数值模拟研究证明软流圈内的小尺度对流对岩石圈底部具有强烈的侵蚀作用, 从而引发岩石圈出现减薄[62], 如华北克拉通东部地区[62,63].

综合上述讨论, 本文发现伊豆-小笠原岛弧地区海洋岩石圈厚度约为62 km, 相对于菲律宾海构造稳定地区海洋岩石圈而言存在减薄现象. 这一减薄应与西太平洋俯冲板块在地球深部持续释放的挥发分物质导致了软流圈出现部分熔融以及弧后地幔楔内小尺度对流的强侵蚀作用密切相关.

**致谢** 感谢美国地震学研究联合会数据管理中心(IRIS DMC)提供的地震波形数据. 感谢中国科学院大学魏荣强副教授和Array Information Technology陈友麟博士对本研究提出的建议. 文中的图件主要采用Generic Mapping Tools绘制.

## 参考文献

1 Gutenberg B. Physics of the Earth's Interior. New York: Academic Press, 1959. 75–97
2 Eaton D W, Darbyshire F, Evans R L, et al. The elusive lithosphere-asthenosphere boundary (LAB) beneath cratons. Lithos, 2009, 1-2: 1–22
3 Fischer K M, Ford H A, Abt D L, et al. The lithosphere-asthenosphere boundary. Annu Res Earth Planet Sci, 2010, 38: 551–575
4 Wei R Q, Li W Y. Thermal-rheological bottom boundary of continental lithosphere: Case studies on cratons of Kaapvaal, Fennoscandia, and Slave (in Chinese). J Univ Chin Acad Sci, 2015, 1: 74–81 [魏荣强, 李午阳. 大陆岩石圈的热-流变底边界——以 Kaapvaal, Fennoscandia 和 Slave 克拉通为例. 中国科学院大学学报, 2015, 1: 74–81]

5 Karato S I, Jung H. Water, partial melting and the origin of the seismic low velocity and high attenuation zone in the upper mantle. Earth Planet Sci Lett, 1998, 3-4: 193–207
6 Naif S, Key K, Constable S, et al. Melt-rich channel observed at the lithosphere-asthenosphere boundary. Nature, 2013, 7441: 356–359
7 Stern R J. Subduction zones. Rev Geophys, 2002, 4: 1012, doi: 10.1029/2001RG000108
8 Tan Y, Helmberger D V. Trans-Pacific upper mantle shear velocity structure. J Geophys Res, 2007, 112: B08301, doi: 10.1029/2006JB004853
9 Romanowicz B. The thickness of tectonic plates. Science, 2009, 324: 474–476
10 Bagley B, Revenaugh J. Upper mantle seismic shear discontinuities of the Pacific. J Geophys Res, 2008, 113: B12301, doi: 10.1029/2008JB005692
11 Kawakatsu H, Kumar P, Shinohara M, et al. Seismic evidence for sharp lithosphere-asthenosphere boundaries of oceanic plates. Science, 2009, 324: 499–502
12 Rychert C A, Shearer P M. A global view of the lithosphere-asthenosphere boundary. Science, 2009, 324: 495–498
13 Schmerr N. The Gutenberg discontinuity: Melt at the lithosphere-asthenosphere boundary. Science, 2012, 327: 1480–1483
14 Kumar P, Kawakatsu H. Imaging the seismic lithosphere-asthenosphere boundary of the oceanic plate. Geochem Geophys Geosyst, 2011, 12: Q01006, doi: 10.1029/2010GC003358
15 Chen L, Cheng C, Wei Z. Seismic evidence for significant lateral variations in lithospheric thickness beneath the central and western North China Craton. Earth Planet Sci Lett, 2009, 1-2: 171–183
16 Shen X, Zhou Y, Zhang Y, et al. Receiver function structures beneath the deep large faults in the northeastern margin of the Tibetan Plateau. Tectonophysics, 2014, 610: 63–73
17 Ai Y, Zheng T, Xu W, et al. A complex 660 km discontinuity beneath northeast China. Earth Planet Sci Lett, 2003, 1-2: 63–71
18 Gao Y, Suetsugu D, Fukao Y, et al. Seismic discontinuities in the mantle transition zone and at the top of the lower mantle beneath eastern China and Korea: Influence of the stagnant Pacific slab. Phys Earth Planet Inter, 2010, 1-2: 288–295
19 Gaherty J B, Kato M, Jordan T H. Seismological structure of the upper mantle: A regional comparison of seismic layering. Phys Earth Planet Inter, 1999, 1-2: 21–41
20 Kato M, Jordan T H. Seismic structure of the upper mantle beneath the western Philippine Sea. Phys Earth Planet Inter, 1999, 3: 263–283
21 Rychert C A, Shearer P M. Imaging the lithosphere-asthenosphere boundary beneath the Pacific using *SS* waveform modeling. J Geophys Res, 2011, 116: B07307, doi: 10.1029/2010JB008070
22 Collier J D, Helffrich G R. Topography of the “410” and “660” km seismic discontinuities in the Izu-Bonin subduction zone. Geophys Res Lett, 1997, 12: 1535–1538
23 Zang S, Zhou Y, Ning J, et al. Multiple discontinuities near 660 km beneath Tonga area. Geophys Res Lett, 2006, 33: L20312, doi: 10.1029/2006GL027262
24 McFadden P L, Drummond B J, Kravis S. The *N*th-root stack: Theory, applications, and examples. Geophysics, 1986, 10: 1879–1892
25 Zhou Y, Yu X, Yang H, et al. Multiplicity of the 660-km discontinuity beneath the Izu-Bonin area. Phys Earth Planet Inter, 2012, 198: 51–60
26 Zang S X, Zhou Y Z. The method of *N*-th root stack and its application in study of mantle discontinuities (in Chinese). Chin J Geophys, 2002, 3: 407–415 [臧绍先, 周元泽. *N* 次根倾斜叠加方法在间断面研究中的应用. 地球物理学报, 2002, 3: 407–415]
27 Flanagan M P, Shearer P M. Topography on the 410-km seismic velocity discontinuity near subduction zones from stacking of *sS*, *sP*, and *pP* precursors. J Geophys Res, 1998, B9: 21165–21182
28 Qin M Z, Zhang Y S, Liu X Z, et al. On “410” discontinuity depth of the Tonga-Fiji subduction zone by the *sP* precursor recorded by Gansu seismic network (in Chinese). Acta Seismol Sin, 2016, 1: 53–58 [秦满忠, 张元生, 刘旭宙, 等. 利用甘肃地震台网记录的 *sP* 前驱波研究汤加-斐济俯冲区“410”间断面深度. 地震学报, 2016, 1: 53–58]
29 Zheng Y, Lay T, Flanagan M P, et al. Pervasive seismic wave reflectivity and metasomatism of the Tonga mantle wedge. Science, 2007, 322: 855–859
30 Wang X R, Li G H, Cui H H, et al. Constraining the discontinuity structure of the upper mantle beneath the Tonga-Fiji subduction zone based on secondary phases (in Chinese). Prog Geophys, 2015, 5: 2089–2099 [王晓冉, 李国辉, 崔辉辉, 等. 基于次生震相的汤加-斐济地区上地幔间断面结构研究. 地球物理学进展, 2015, 5: 2089–2099]
31 Wu S G, Fan J K, Dong D D. Discussion on the tectonic division of the Phillippine Sea Plate (in Chinese). Chin J Geol, 2013, 3: 677–692 [吴时国, 范建柯, 董冬冬. 论菲律宾海板块大地构造分区. 地质科学, 2013, 3: 677–692]
32 Helffrich G. Topography of the transition zone seismic discontinuities. Rev Geophys, 2000, 1: 141–158
33 Rost S, Thomas C. Array seismology: Mehod and applications. Rev Geophys, 2002, 3: 2-1–2-27
34 Zhou Y Z, Wang Z J. On the difference of mid-mantle multiple velocity structure beneath Izu-Bonin and Tonga areas (in Chinese). Sci Sin Terr, 2011, 7: 936–944 [周元泽, 王卓君. 伊豆-小笠原和汤加地区中地幔多层速度结构差异性研究. 中国科学: 地球科学, 2011, 7: 936–944]

35 Kanasewich E R, Alpaslan T, Hemmings C D. *N*th-root stack nonlinear multichannel filter. Geophysics, 1973, 2: 327–338

36 Li J, Chen Q, Vanacore E, et al. Topography of the 660-km discontinuity beneath northeast China: Implications for a retrograde motion of the subducting Pacific slab. Geophys Res Lett, 2008, 35: L01302, doi: 10.1029/2007GL031658

37 Schimmel M, Paulssen H. Noise reduction and detection of weak, coherent signals through phase-weighted stacks. Geophys J Int, 1997, 2: 497–505

38 Amante C, Eakins B W. ETOPO1: 1 arc-minute global relief model: Procedures, data sources and analysis. NOAA Technical Memorandum NESDIS NGDC-24. National Geophysical Data Center, NOAA, 2009, doi: 10.7289/V5C8276M

39 Ekström G, Nettles M, Dziewoński A M. The global CMT project 2004–2010: Centroid-moment tensors for 13017 earthquakes. Phys Earth Planet Inter, 2012, 200-201: 1–9

40 Dziewonski A M, Chou T A, Woodhouse J H. Determination of earthquake source parameters from waveform data for studies of global and regional seismicity. J Geophys Res, 1981, B4: 2825–2852

41 Wang R. A simple orthonormalization method for stable and efficient computation of Green's functions. Bull Seismol Soc Amer, 1999, 3: 733–741

42 Laske G, Masters G, Ma Z, et al. CRUST1.0: An updated global model of Earth's crust. EGU General Assembly, 2012, 14: 3743

43 Kennett B L N, Engdahl E R. Traveltimes for global earthquake location and phase identification. Geophys J Int, 1991, 2: 429–465

44 Crotwell H P, Owens T J, Ritsema J. The TauP toolkit: Flexible seismic travel-time and ray-path utilities. Seismol Res Lett, 1999, 2: 154–160

45 Buland R, Chapman C H. The computation of seismic travel times. Bull Seismol Soc Amer, 1983, 5: 1271–1302

46 Chen J, Zhou Y Z, Wang H C. Detection of the Lehmann discontinuity beneath Tonga with short-period waveform data from Hi-net (in Chinese). Sci Sin Terr, 2014, 7: 1468–1476 [陈健, 周元泽, 王红才. 基于 Hi-net 短周期地震波形资料的汤加地区 Lehmann 间断面研究. 中国科学: 地球科学, 2014, 7: 1468–1476]

47 Chen L, Jiang M, Yang J, et al. Presence of an intralithospheric discontinuity in the central and western North China Craton: Implications for destruction of the craton. Geology, 2014, 3: 223–226

48 Karato S I. On the origin of the asthenosphere. Earth Planet Sci Lett, 2012, 321-322: 95–103

49 Selway K, Ford H, Kelemen P. The seismic mid-lithosphere discontinuity. Earth Planet Sci Lett, 2015, 414: 45–57

50 Vinnik L, Niu F, Kawakatsu H. Broadband converted phases from midmantle discontinuities. Earth Planet Space, 1998, 11: 987–997

51 Niu F, Kawakatsu H, Fukao Y. Seismic evidence for a chemical heterogeneity in the midmantle: A strong and slightly dipping seismic reflector beneath the Mariana subduction zone. J Geophys Res, 2003, 108: 2419, doi: 10.1029/2002JB002384

52 Yang Z, He X. Oceanic crust in the mid-mantle beneath west-central Pacific subduction zones: evidence from *S* to *P* converted waveforms. Geophys Res Lett, 2015, 1: 541–547

53 Gudmundsson Ó, Sambridge M. A regionalized upper mantle (RUM) seismic model. J Geophys Res, 1998, B4: 7121–7136

54 Turcotte D L, Schubert G. Geodynamics. 2nd ed. Cambridge: Cambridge University Press, 2002. 285–290

55 Ishizuka O, Kimura J I, Li Y B, et al. Early stages in the evolution of Izu-Bonin arc volcanism: New age, chemical, and isotopic constraints. Earth Planet Sci Lett, 2006, 1-2: 385–401

56 Artemieva I M. The Lithosphere: An Interdisciplinary Approach. New York: Cambridge University Press, 2011. 1–14

57 Zang S X, Ning J Y. Study on the subduction zone in western pacific and its implication for the geodynamics (in Chinese). Chin J Geophys, 1996, 2: 188–202 [臧绍先, 宁杰远. 西太平洋俯冲带的研究及其动力学意义. 地球物理学报, 1996, 2: 188–202]

58 Huang J, Zhao D. High-resolution mantle tomography of China and surrounding regions. J Geophys Res, 2006, 111: B09305, doi: 10.1029/2005JB004066

59 Fukao Y, Obayashi M. Subducted slabs stagnant above, penetrating through, and trapped below the 660 km discontinuity. J Geophys Res, 2013, 11: 5920–5938

60 Lei J, Xie F, Fan Q, et al. Seismic imaging of the deep structure under the Chinese volcanoes: An overview. Phys Earth Planet Inter, 2013, 224: 104–123

61 Zhao D, Maruyama S, Omori S. Mantle dynamics of western Pacific and east Asia: Insight from seismic tomography and mineral physics. Gondwana Res, 2007, 1: 120–131

62 He L. Numerical modeling of convective erosion and peridotite-melt interaction in big mantle wedge: Implications for the destruction of the North China Craton. J Geophys Res-Solid Earth, 2014, 119: 3662–3677

63 Zhu G, Shi Y, Tackley P. Subduction of the western Pacific plate underneath northeast China: Implications of numerical studies. Phys Earth Planet Inter, 2010, 1: 92–99

Summary for “伊豆-小笠原地区岩石圈软流圈边界地震学证据”

# Seismic evidence of the lithosphere-asthenosphere boundary beneath Izu-Bonin area

CUI HuiHui[1,2], GAO YaJian[1,2] & ZHOU YuanZe[1,2*]

[1] *Key Laboratory of Computational Geodynamics, Chinese Academy of Sciences, Beijing 100049, China;*
[2] *College of Earth Science, University of Chinese Academy of Sciences, Beijing 100049, China*
* Corresponding author, E-mail: yzzhou@ucas.ac.cn, yzzhou@gmail.com

The lithosphere-asthenosphere boundary (LAB) is the seismic discontinuity with the negative velocity contrast in the upper mantle. The plate tectonic theory describes that the rigid lithosphere translate coherently over the ductile asthenosphere, and the LAB implies the decoupling between the two layers. The seismic velocity, viscosity, electrical resistivity and other physical parameters change with the depths across the boundary. The LAB has become a focus of seismology studies for its significance in understanding the plate motions, the mantle convection and the lithospheric evolution processes. Seismic detections on the LAB in subduction zone areas are helpful to understand the interactions between the lithosphere and asthenosphere layers and the geodynamic processes related with the slab subductions. For the dense permanent networks and transportable arrays of the USArray, the abundant waveforms of the deep earthquake events beneath the Izu-Bonin area can be recorded and retrieved. In this study, the vertical broadband waveforms are collected from three earthquake events occurring from 2002 to 2014 with the focal depths of 400–600 km. The source parameters are taken from the Preliminary Determinations of Epicenters catalog of US Geological Survey, and the focal fault solutions are taken from the global Centroid-Moment-Tensor project. The seismic waveforms are manually selected with two criteria: (1) simple *sP* arrivals with clear peaks, and (2) high signal-to-noise ratios and without abnormal spikes. In order to enhance the weak unknown precursors, the linear slant stack method, which is the special form of the *N*-th root slant stack method and phase-weighted stack method, is applied to scan the differential slowness and stack the seismograms in the domain of differential travel-time and differential slowness. The selected waveform data is processed to obtain the vespagrams and the stacked waveforms. The *sP* precursors reflected on the LAB ($s_{\mathrm{LAB}}P$), which have the opposite polarities with the amplitude ratios of 0.17–0.21 relative to the *sP* phases, are successfully extracted in our results. To reduce the possible effects of the crustal structures on the propagations of *sP* phases, the one-dimensional modified velocity model (IASP91-IB) is established by replacing the crust part of the IASP91 model with the CRUST1.0 model. On the basis of the modified model, we obtain the distributions for six reflected points of the $s_{\mathrm{LAB}}P$ phases near the source area. Our results reveal that the LAB depths range between 58 and 65 km beneath the Izu-Bonin Arc, with the average depth of 62 km and the small topography of 7 km. Based on the half-space cooling model for the oceanic lithosphere, the lithosphere beneath the Izu-Bonin Arc is about located at the isotherm of 950°C, and the lithosphere beneath the West Philippine Basin (WPB) and Parece Vela Basin (PVB) is about located at the isotherm of 1100°C. Compared with the results of the tectonic stable areas (WPB and PVB) in the Philippine Sea, the lithosphere beneath the Izu-Bonin Arc shows the obvious thinning phenomenon. The numerical modeling experiments have revealed the strong erosions of the convecting asthenosphere in the mantle wedge, resulting in the destruction of the craton. We infer that the lithospheric thinning beneath the Izu-Bonin Arc is closely related with the partial melting, which is caused by the volatiles continuously released from the subducted western Pacific slab, and the strong erosions of the small-scale mantle convections in the back-arc mantle wedge.

**lithosphere-asthenosphere boundary, Izu-Bonin area, subduction zone, *sP* precursors, linear slant stack**

doi: 10.1360/N972016-00889